SPIE's 10th Annual International Symposium on Smart Structures and Materials and 8th Annual International Symposium on NDE for Health Monitoring and Diagnostics, 2-6 March 2002, San Diego, CA. paper # 5047-15

Comparative Study of Neural-Network Damage Detection from a Statistical Set of Electro-Mechanical Impedance Spectra

Victor Giurgiutiu, PhD
Mechanical Engineering Department, University of South Carolina
Columbia, SC 29208, victorg@sc.edu

Claudia Kropas-Hughes, PhD
NDE Research Leader, Air Force Research Lab, Materials and Manufacturing Directorate,
AFRL/MLLP, 2230 Tenth Street, Wright-Patterson AFB, OH 45433,
Claudia.Hughes@wpafb.af.mil

ABSTRACT

The detection of structural damage from the high-frequency local impedance spectra is addressed with a spectral classification approach consisting of features extraction followed by probabilistic neural network pattern recognition. The paper starts with a review of the neural network principles, followed by a presentation of the state of the art in the use of pattern recognition methods for damage detection. The construction and experimentation of a controlled experiment for determining benchmark spectral data with know amounts of damage and inherent statistical variation is presented. Spectra were collected in the 10–40 kHz, 10–150 kHz, and 300–450 kHz for 5 damage situations, each situation containing 5 members, ”identical”, but slightly different. A features extraction algorithm was used to determine the resonance frequencies and amplitudes contained in these high-frequency spectra. The feature vectors were used as input to a probabilistic neural network. The training was attained using one randomly selected member from each of the 5 damage classes, while the validation was performed on all the remaining members. When features vector had a small size, some misclassifications were observed. Upon increasing the size of the features vector, excellent classification was attained in all cases. Directions for further studies include the study of other frequency bands and different neural network algorithms.

Keywords: structural health monitoring, probabilistic neural networks, active sensors, spectral classification, piezoelectric, aging aircraft, cracks, damage, faults, diagnostics, prognostics, PWAS, PNN, E/M impedance

1. INTRODUCTION

Structural Health Monitoring is a major component of the Integrated Vehicle Health Monitoring thrust within the Robust Aerospace Vehicle concept, as envisaged by AFRL, ONR, NASA, and industry (Kropas-Hughes, 2002a). The electro-mechanical (E/M) impedance approach permits the direct measurement of the high-kHz drive-point mechanical impedance spectrum as seen by a piezoelectric wafer active sensor (PWAS) mounted on the examined structure. In thin-wall structures, high-kHz excitation generates standing Lamb waves that represent localized structural modes, which are highly sensitive to incipient damage. In addition, due to the high-kHz bandwidth, such spectra are impervious to noise and disturbances originating from normal aircraft operation, because such noise and disturbances characteristically happen at much lower frequencies. Thus, the E/M impedance method offers good opportunities for identification of incipient local damage during the vehicle structural health monitoring process. The determination of damage presence from the high kHz impedance spectra, though in principle possible, is however challenging. At high kHz, the resonance spectra of thin wall structures contain a large number of harmonics, each of them being differently affected by the damage presence. Beside the expected frequency shifts, the appearance of new peaks, and the splitting of existing peaks has also been observed. Therefore, the study of such spectral changes, and the classification of spectra with various amounts of damage are best approached with statistical pattern recognition methods and neural network algorithms.

Report Documentation Page

Form Approved
OMB No. 0704-0188

1. REPORT DATE	2. REPORT TYPE	3. DATES COVERED
2002	**N/A**	**-**

4. TITLE AND SUBTITLE	5a. CONTRACT NUMBER
Comparative Study of Neural-Network Damage Detection from a Statistical Set of Electro-Mechanical Impedance Spectra	5b. GRANT NUMBER
	5c. PROGRAM ELEMENT NUMBER
6. AUTHOR(S)	5d. PROJECT NUMBER
	5e. TASK NUMBER
	5f. WORK UNIT NUMBER
7. PERFORMING ORGANIZATION NAME(S) AND ADDRESS(ES) **University of South Carolina, Mechanical Engineering Department Columbia, SC 29208**	8. PERFORMING ORGANIZATION REPORT NUMBER
9. SPONSORING/MONITORING AGENCY NAME(S) AND ADDRESS(ES)	10. SPONSOR/MONITOR'S ACRONYM(S)
	11. SPONSOR/MONITOR'S REPORT NUMBER(S)

12. DISTRIBUTION/AVAILABILITY STATEMENT
Approved for public release, distribution unlimited

13. SUPPLEMENTARY NOTES
The original document contains color images.

14. ABSTRACT

15. SUBJECT TERMS

16. SECURITY CLASSIFICATION OF:			17. LIMITATION OF ABSTRACT	18. NUMBER OF PAGES	19a. NAME OF RESPONSIBLE PERSON
a. REPORT	b. ABSTRACT	c. THIS PAGE			
unclassified	**unclassified**	**unclassified**	**UU**	**12**	

2. NEURAL NETWORKS

Neural Networks are biologically inspired artificial intelligence representations that mimic the functionality of nervous systems (Bishop, 1995; Cowell et al. 1999; Demuth and Beale, 2000). Biological neurons consist of **synapses**, **dendrites**, **axons**, and **cell bodies**. Specific to the biological neuron is there ability to **fire** when **activated**. Artificial neurons are on-off device, which are set on by the **activation** or **transfer function** (a.k.a. **threshold function**). The activation function $g(\bullet)$ can be discontinuous (e.g., symmetrized Heaviside step function, a.k.a. **hardlimit)**, or continuous (e.g., logistic sigmoid, a.k.a. **logsig).** Linear transfer function are also be used. In an artificial **neural network,** each simulated neuron is viewed as a node connected to other nodes (neurons) through **links** to form a network. Each link is associated to a **weight**. The weight determines the nature and strength of one neuron's influence on another. Neural networks are organized in layers, **input layer**, **output layer,** and **hidden layers**. (The output of the neurons in hidden layers is not observable from the outside world.) Artificial neural networks consist of **multipliers**, **adders**, and **transfer functions.** They can be implemented as software algorithms and/or hardwired electronic device. Currently, artificial neural network algorithms are widely available as software packages (Hagan et al., 1996; Demuth and Beale, 2000).

2.1 Types of Artificial Neural Network

Some common neural network types are: (a) **feedforward**; (b) **Autoassociative/heteroassociative;** (c) **recurrent;** (d) **competitive;** (e) **probabilistic**.

Feedforward neural networks compute the output directly from the input, in one pass. No feedback is involved. Feed-forward networks can recognize regularity in data; they can serve as pattern identifiers. A typical feedforward neural network is the **perceptron.** The perceptron scalar output equals 1 when a pattern has been identified, and 0 otherwise. The mathematical representation of the perceptron is

$$y(\mathbf{x}) = g\left(\sum_{i=0}^{N} w_i x_i\right) = g(\mathbf{w}^T \mathbf{x}) \,, \tag{1}$$

where $g(\bullet)$ is the output transfer function, and x_0 is always set to 1 ($x_0 = 1$) such that w_0 plays the role of bias. A generalized perceptron uses nonlinear transfer functions, $\phi_j(\bullet)$, a.k.a., **basis functions,** which are placed between the input and the adder:

$$y(\mathbf{x}) = g\left(\sum_{i=0}^{N} w_i \phi_i(\mathbf{x})\right) = g\left(\mathbf{w}^T \boldsymbol{\varphi}(\mathbf{x})\right). \tag{2}$$

Interconnected perceptrons form **perceptron layers.** Several perceptron layers lead to a **multi-layer perceptron** neural network. In pattern recognition, multi-layer feedforward neural networks can identify **class separation boundaries** in the form of **hyper-planes** in the multidimensional input space (Figure 2a).

Autoassociative neural networks (AANN) are feedforward artificial neural networks generated from multi-layer perceptrons. AANN have been extended from processing one dataset to processing two datasets simultaneously. These are referred to as heteroassociative neural networks (HANN) and map one dataset on the input to a target dataset at the output that is different from the input. The HANN can effectively generate a second dataset from the first dataset. Another type of HANN is a network with both datasets as input and output. This joint data HANN provides for a mutual mapping of the two datasets. The autoassociative-heteroassociative neural network (A-HANN) provides the ability to predict one dataset from another dataset and, at the same time, validate the accuracy of the predicted dataset (Kropas-Hughes et al., 2002b).

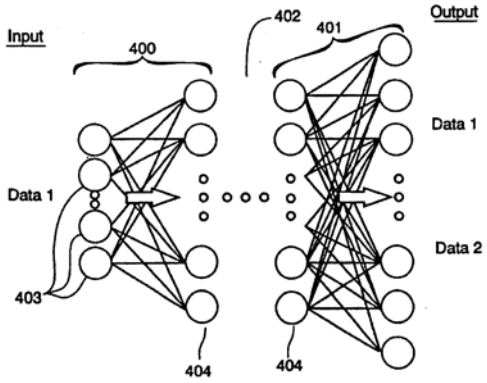

Figure 1 Autoassociative-heteroassociative neural network (Kropas-Hughes et al, 2002b)

Recurrent neural networks have feedback connections from output to the input. They can learn to identify a pattern. A typical recurrent network is the **Hopfield network**, which can be easily hardwired using resistors, capacitors, and feedback connections. They have been used for associative memories, and optimization problems. The output of a Hopfield network is the very pattern that was identified.

Competitive neural networks are characterized by two properties: (a) they compute some measure of the distance between stored prototype patterns and the input pattern; and (b) they perform a competition between the output neurons to determine which neuron represents the prototype pattern closest to the input. **Adaptive competitive neural networks** adjust the prototype patterns as new inputs are applied to the neural network. Thus, an adaptive competitive neural network learns to cluster inputs into different input classes. A typical competitive network is the two-layer **Hamming network**. The first layer is a **feedforward network**, while the second layer is a **recurrent network** that performs the neuron competition and determines a winner. The output of a Hamming network is a vector containing a "1" at a row position corresponding to the identified class.

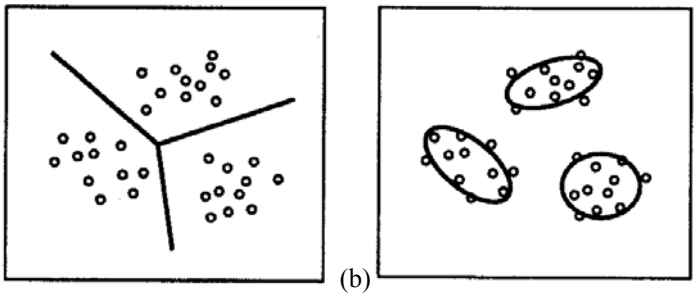

Figure 2 Separation of features vectors into class clusters: (a) a multi-layer perceptron yields straight boundaries (hyperplanes); (b) radial basis neural networks yields curved enclosures for each class (Bishop, 1995)

Probabilistic neural networks are hybrid multi-layer networks that use basis functions and competitive selection concepts. Probabilistic neural network achieve a Bayesian decision analysis with Gaussian kernel (Parzan window). A probabilistic neural network consists of a **radial-basis layer**, a **feedforward layer**, and a **competitive layer**. The radial basis functions depend on the distance between the input vectors and some **prototype vectors,** $\boldsymbol{\mu}_j$, representative of the various input classes.

$$y_k(\mathbf{x}) = \sum_{m=0}^{M} w_{km}\phi_m(\mathbf{x}), \qquad \phi_m(\mathbf{x}) = \exp\left(-\frac{\|\mathbf{x}-\boldsymbol{\mu}_m\|^2}{2\sigma_m^2}\right), \ \phi_0 = 1 \tag{3}$$

Probabilistic neural networks identify class separation boundaries as **hyper-spheres** in the input space (Figure 2b).

2.2 Training of Neural Networks

Multi-layer feedforward neural networks are trained through **backpropagation,** which is a generalized learning rule for neural networks with nonlinear differentiable transfer functions. The method is called *backpropagation* because it computes first the changes to the weights in the final layer, and then reuses much of the same computation to calculate the changes to the weights in the penultimate layer, and so on until it reaches *back* to the initial layer. Standard backpropagation uses the gradient descent algorithm; other optimization techniques such as Newton-Raphson, conjugate gradients, etc. have also been used.

The training through backpropagation is **iterative**, and can take several presentations of the training set. During training, the weights are optimized by minimization of a suitable error function, e.g., the sum-of-squared-errors $E = \frac{1}{2}\sum_n \sum_k \left\{ y_k(\mathbf{x}^n; w_{kj}) - t_k^n \right\}^2$. The backpropagation training has an **exit strategy**, i.e., the training is stopped when the output error falls below given **convergence thresholds**. The duration of learning depends considerably on the **rate parameter** (a.k.a. regularization parameter) which controls the changes made to the neural network weights after each training cycle. The rate parameter controls the step size in the gradient descent; hence, if the step size is large, non-linear effects become significant, and strongly affect the validity of the gradient calculation formulae. If the training is too long, the network becomes too specialized on the training data and looses generalization, i.e. has unsatisfactory performance on validation data. A method for improving generalization is **early stopping**.

Probabilistic neural networks are trained in two stages:

The *first stage* consists of **unsupervised learning.** In the first stage, the training input vectors, $\mathbf{x}^n$, are used to determine the basis-function parameters, $\boldsymbol{\mu}_j$ and σ_j. Either an **exact design** or an **adaptive design** can be used. The exact design sets the prototype vectors equal to the input training vectors, $\boldsymbol{\mu}_j = \mathbf{x}^n$, $j = n$. The adaptive design clusters the input vectors and determines prototype vectors that are representative of several input vectors. One way of implementing the adaptive design is through incremental addition of neurons. Radial basis neurons are added until the sum-squared error falls beneath an error goal, or a predetermined number of neurons is reached. At each iteration, if an input vector results in lowering the network error, then it is used to create a new radial-basis neuron. The radial spread parameters, σ_j, are adjusted to achieve optimal coverage of the input space.

The *second stage* consists of **supervised learning.** In the second stage, the basis functions are kept fixed (matrix **Φ),** and the linear-layer weights, w_{nj}, are found to fit the training output values, $\mathbf{t}^n$, using backpropagation. The formal solution for the weight is given by: $\mathbf{W} = \left(\mathbf{\Phi}^{\dagger}\mathbf{T}\right)^T$ where $\mathbf{\Phi}^{\dagger}$ denotes the pseudo-inverse of **Φ**. In practice, this is solved using the singular value decomposition to avoid problems due to the possible ill conditioning of matrix **Φ**. Figure 4a presents a simple probabilistic network classification example (Demuth and Beagle, 2000). The training vectors $\mathbf{x}_1$, $\mathbf{x}_2$, $\mathbf{x}_3$, $\mathbf{x}_4$, $\mathbf{x}_5$, $\mathbf{x}_6$, $\mathbf{x}_7$, were used to train the neural network and define the classes 1, 2, and 3. Then, the new vectors **α, β, γ**, were used to perform validation of the neural network. The new vectors were successfully assigned. Figure 4b presents the general architecture of the probabilistic neural network.

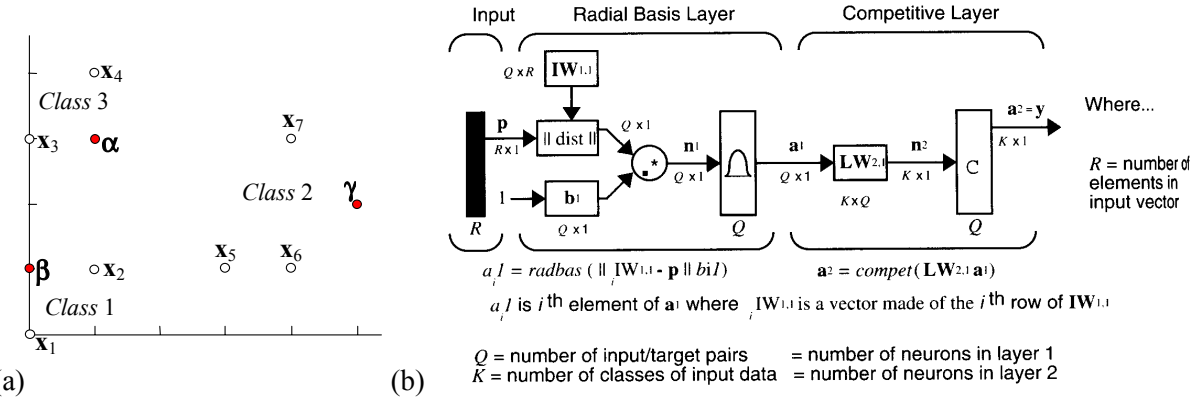

Figure 3 Classification using probabilistic neural networks: (a) $\mathbf{x}_1$, $\mathbf{x}_2$, $\mathbf{x}_3$, $\mathbf{x}_4$, $\mathbf{x}_5$, $\mathbf{x}_6$, $\mathbf{x}_7$ are the training vectors defining classes 1, 2, and 3 and **α, β, γ** are the new vectors that have been classified; (b) the general architecture of of probabilistic neural network (Demuth and Beale, 2000)

3. PATTERN-RECOGNITION METHODS FOR DAMAGE IDENTIFICATION

Automatic pattern recognition plays a preeminent role in artificial intelligence research (Winston, 1993). Early successes obtained with automatic chemical classification (e.g., the DENDRAL mass spectrogram analyzer, Lindsay et al., 1980) and medical inference (e.g., the MYCIN bacterial diagnosis expert system, Shotliffe and Buchanan, 1975) spurred the research interest in this field. Figure 4 presents the typical steps of a pattern recognition process: A sensor transforms the physical state into a measured signal. The preprocessor removes unnecessary or corrupting information from the signal. The feature extractor computes the features required for classification. The classifier yields a decision regarding the class membership of the pattern being analyzed, i.e., achieve the pattern-recognition goal.

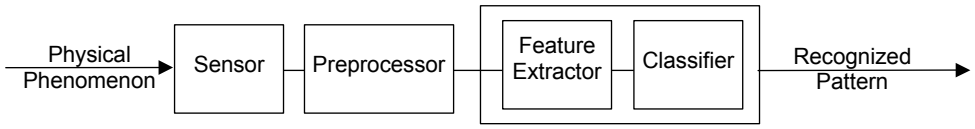

Figure 4 Schematic of a pattern recognition process (after Winston, 1993)

Farar et al. (2001) pointed out that statistical modeling for feature discrimination uses algorithms that analyze distributions in the features spaces in order to determine the damage state of the structure. Statistical modeling is used to quantify when changes in data features can be considered significant. In addition, such algorithms can be used to discriminate between changes caused by damage and changes caused by varying operational and environmental conditions. Statistical modeling algorithms fall into three general categories: (1) group classification, (2) regression analysis, (3) outlier detection. The appropriate algorithm will depend on the ability to perform supervised and unsupervised learning. The latter involves statistical process control, principal component analysis, and linear or quadratic discriminants. Building on statistical and adaptive signal processing (Manolakis et al., 2000), recent automatic pattern recognition research has focused on using artificial neural networks (Nigrin, 1993; Bishop, 1995; Mehrotra et al., 1997; Looney, 1997; Omidvar and Dayhoff, 1998; Cowell et al., 1999; Principe et al., 2000).

3.1 Neural Networks for Structural Damage Identification

Extensive modal-analysis studies have focused on using automatic pattern recognition method for structural damage identification from modal-analysis spectral data. Worden (2000) reviewed the use of multi-layer perceptron and radial basis function neural networks and genetic algorithms for modeling the time response of a nonlinear Duffing oscillator with hysteretic response. Worden et al. (2000) studied two structural health-monitoring methods, the first performing novelty detection on the low-frequency (0–250 Hz) transmissibility, the second extracting frequencies and modeshapes, and quantifying a damage index. Farar et al. (1999), Ying et al. (2001), Jin et al. (2001) considered statistical pattern recognition method for vibration based structural health monitoring using stochastical analysis. Zang and Imregun (2000) used damage detection with a neural network that recognizes specific patterns in a compressed frequency response function (FRF). The compression of the FRF data was achieved with a principal component analysis algorithm. Chan et al. (1999) used neural network novelty filtering to detect anomaly in bridge cables using the measured frequency of the cables. Ni et al. (2001) studied the application of adaptive probabilistic neural network to suspension bridge damage detection. Sohn et al. (2001) studied the novelty detection under changing environmental conditions. Sohn and Farar (2000), Todoroki et al. (1999), Loh and Huang (1999), Lloyd and Wang (1999), Liu et al. (1999) studied the statistical and neural network processing of time-domain signals. Chang et al. (1999), Ho and Ewins (1999); Hu and Fukunaga (2001) followed the model-based approach to structural damage detection. Fritzen and Bohle (1999) studied parameter selection strategies for modal-analysis damage detection using the experimental data collected during the controlled experiments on the I-40 bridge over the Rio Grande, New Mexico. Modal analysis measurements in the range 2-12 Hz were collected at 26 accelerometer locations. An initial cut (600 mm long by 10mm wide), was progressively expanded until it completely cut through the bridge. However, positive detection was only possible when the cut had almost passed through the frame, highlighting the difficulty of detecting incipient damage with low-frequency modal analysis.

3.2 Classification of E/M Impedance High-frequency Spectra

A promising technique for damage detection using spectral comparison is the electromechanical (E/M) impedance method. Pioneered by Liang *et al.* (1994), this method has the marked advantage of being able to measure the high-frequency (hundreds of kHz) local impedance data in the near field of a piezoelectric wafer active sensor (PWAS) attached to the structure. Thus, it can measure with ease the high order harmonics, which are more sensitive to local damage than the low order harmonics. As shown theoretically and experimentally by Giurgiutiu and Zagrai (2000, 2002), the local impedance spectrum of the structure is reflected directly in the real part of the E/M impedance of the PWAS attached to the structure. The ability to directly measure the local structural impedance at high frequency is essential for the early detection of incipient damage that will affect the high-frequency local modes, but will not be able to influence the low-frequency global modes considered in conventional modal analysis. Thus, the use of high frequencies ensures that the damage metric detects incipient damage at an early stage. Two approaches have emerged for the classification of an entire spectrum: (a) overall-statistics methods, and (b) features-based methods. **Overall-statistics methods** are easier to use, since they attempt to directly compare the strings of numbers associated with each spectrum using simple statistical formulae. Such methods may be appropriate for the classification of E/M impedance spectra measured of massive highly damped structures, such as in the identification of delaminations of composite overlays applied to concrete or brick structures. In this case, the E/M impedance spectrum of the pristine structure has few shallow resonances, while the spectrum of the delaminated structure will have a marked new peak. However, the overall-statistics methods have been shown ineffective for the classification of high-frequency spectra of lightly damped thin-wall structures that have many resonance peaks, which shift, split, and multiply when local damage appears. In this case, feature-based methods are more appropriate.

The **feature-based methods** use a two-stage approach: first, the spectral features that are likely to be affected by damage are extracted. In this first step, the problem dimensionality is reduced by at least an order of magnitude. In the second step, the features vectors associated with each spectrum are compared using a vector classification technique. Early attempts to use this technique for the classification of E/M impedance spectra using neural network techniques were reported by Lopes and Inman (1999), and Lopes et al. (1999). In analytical simulations, a three level normalization scheme was applied to the E/M impedance spectrum base on the resonance frequencies. First, the sensitivity of certain resonance frequencies to the location of the damage was identified. Second, the excursion of the frequency change with damage amplitude at each location was calculated. Thirdly, the normalized percentage frequency change for each damage severity was calculated. One-layer and two-layer neural networks were constructed and successfully trained on analytical models with simulated damage. But when applied to actual experiments, e.g., a 4-bay bolted structure and a 3-bay screw-connected space frame, this neural network approach

did not work, and had to be modified. Another set of normalized values were used: (i) the area between damaged and undamaged impedance curves; (ii) the root mean square (RMS) of each curve; and (iii) the correlation coefficient between damaged and undamaged curves. These values were calculated for both real and imaginary parts of the impedance spectrum. However, these early attempts were not very conclusive. It seems that before applying spectral classification techniques to actual structures, a good understanding of the likely effects that the damage would have on the spectra is needed. Carefully conducted calibration experiments, in which the effect of damage on the local impedance spectrum is well understood and quantified, have been performed on circular plate specimens with various amounts of damage. The effect of the statistical variations inherent in any fabrication and operation process was also assessed and compared with the damage effects. Thus, a detection threshold calibrated against the statistical "background noise" would be established, to be used in damage detection on actual structures. This paper presents the results of such statistically controlled calibration experiments

4. STATISTICALLY-CONTROLLED CALIBRATION EXPERIMENTS

Controlled structural health monitoring experiments were conducted to generate consistent benchmark test data for damage metrics development and calibration. Five statistical groups of specimens with increasing amount of damage were tested. Each group contained five 1.6-mm thick 2024-T3 aluminum alloy 100-mm diameter identical plates. A 7-mm diameter, 0.2-mm thick piezoelectric-wafer active sensor (PWAS) was placed in the center. A 10-mm simulated crack was produced in each specimen in the form of a curved narrow slit cut with the electric discharge machining (EDM) process (Figure 5). The crack was incrementally brought closer to the plate center (Table 1, column 1). Each crack position represented a different state of damage. Group 0 represented the *pristine* condition. The amount of damage increased as the group number increased. Within each group, the damage was identically replicated to all the group members. Thus, the method's repeatability and reproducibility was tested. An HP 4194A Phase-Gain Impedance Analyzer was used to measure the E/M impedance at the PWAS terminals. The local mechanical impedance of the structure was obtained directly from the real part of the measured E/M impedance. Measurements were performed at 400 frequency points, equally spaced in a preselected frequency band. Three high-frequency bands were used: 10–40 kHz; 10–150 kHz; and 300–450 kHz. The 10–40 kHz frequency band, which has fewer modes, is shown in column 2 of Table 1. As damage progressed, three phenomena occurred:

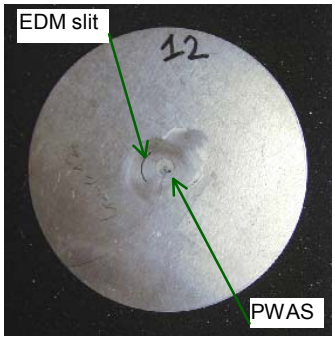

Figure 5 Typical specimen

(a) Resonance peaks shift
(b) Some resonance peaks split
(c) New resonance peaks appear

These changes are apparent by visual inspection of the 10–40 kHz spectra presented in column 2 of Table 1. Similar results were also obtained for the other two frequency bands. The third column of Table 1 gives the values of the six most prominent resonance frequencies of the low-frequency spectra recorded for each of the five plates in the group. It is apparent that the frequencies are nominally the same, but inherent statistical variations are present.

4.1 Inherent Statistical Variation of the Impedance Data

Knowledge of the statistical variation existent in nominally identical situations is of great importance for the assessment and calibration of any health monitoring method. During our experiments, attention was given to producing nominally "identical" specimens. However, slight variations were unavoidable, giving rise to random error in the E/M impedance data. Such variations may be due to geometric tolerances on specimen fabrication, or to positioning of the PWAS transducer on the specimen. Variations due to geometric tolerances would produce shifts in the resonance frequencies, while PWAS positioning variations would dictate which modes are excited. Since the specimen is a circular plate with axial symmetry, a PWAS exactly positioned in the plate center would excite only the axisymmetric modes, while a PWAS ever so slightly displaced from the center will also excite non-axisymmetric modes. Figure 6 illustrates these aspects in the 10–40 kHz band. Three type of modes are observed:

(i) Axisymmetric flexural modes (AF)
(ii) Axisymmetric radial modes (AR)
(iii) Non-axisymmetric modes (NA)

Table 1 Calibration experiments on circular plates

Group 0
(pristine).
5 Plates with no cracks

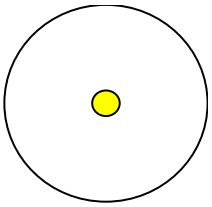

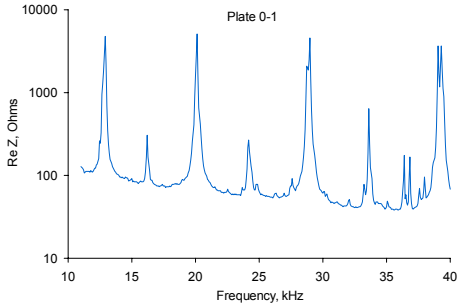

#		1	2	3	4	5
		Plate 0-1	Plate 0-2	Plate 0-3	Plate 0-4	Plate 0-5
Frequency, Hz	f_1	12885	12740	13030	12885	12740
	f_2	16220	16075	16510	16148	16148
	f_3	20135	19918	20425	20135	19918
	f_4	24195	23978	24630	24413	24050
	f_5	28980	28618	29343	28980	28618
	f_6	39058	38913	39493	39493	38913

Group 1
(slight damage)
5 plates with crack at 40mm

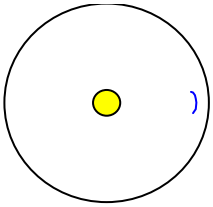

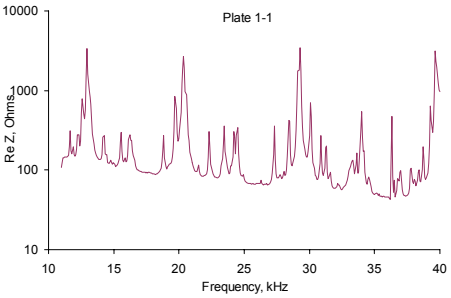

#		6	7	8	9	10
		Plate 1-1	Plate 1-2	Plate 1-3	Plate 1-4	Plate 1-5
Frequency, Hz	f_1	12958	12813	12813	12813	12813
	f_2	19700	19555	19555	19483	19483
	f_3	20353	20135	20063	20063	20063
	f_4	28400	28183	28183	28183	28183
	f_5	29270	28980	28835	28908	28835
	f_6	39638	39203	39203	39203	39130

Group 2
(intermediate damage I)
5 plates with crack at 25mm

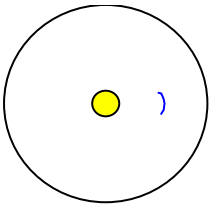

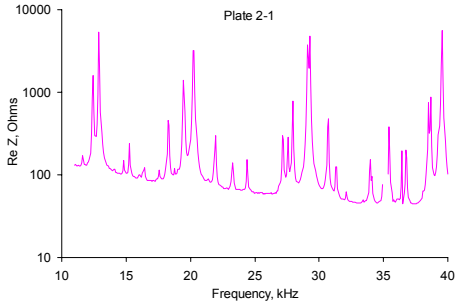

#		11	12	13	14	15
		Plate 2-1	Plate 2-2	Plate 2-3	Plate 2-4	Plate 2-5
Frequency, Hz	f_1	12450	12450	12523	12450	12523
	f_2	12885	12885	13030	12958	12958
	f_3	20280	20135	20353	20208	20353
	f_4	27965	27893	28038	27893	27965
	f_5	29270	28980	29343	29198	29198
	f_6	39565	39348	39783	39348	39710

Group 3
(intermediate damage II)
5 plates with crack at 10mm

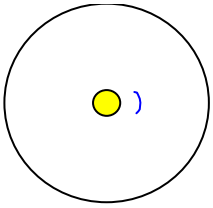

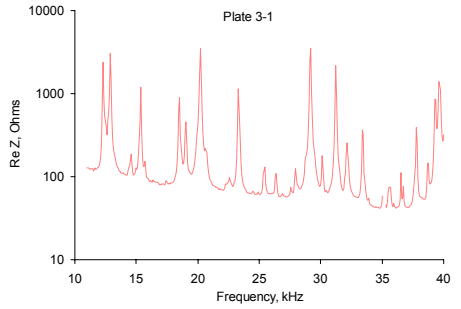

#		16	17	18	19	20
		Plate 3-1	Plate 3-2	Plate 3-3	Plate 3-4	Plate 3-5
Frequency, Hz	f_1	12305	12160	12233	12233	12160
	f_2	12885	12813	12885	12958	12740
	f_3	20208	19990	20135	20135	19990
	f_4	23325	23108	23325	23253	23108
	f_5	29198	28908	29053	28980	28835
	f_6	39638	39348	39565	39493	39203

Group 4
(strong damage)
5 plates with crack at 3mm

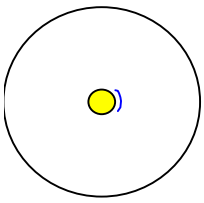

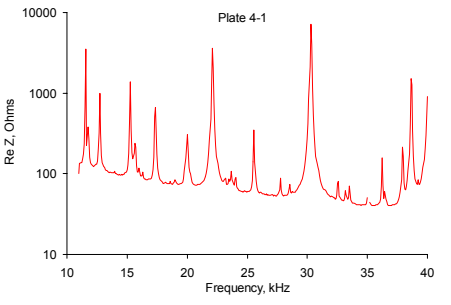

#		21	22	23	24	25
		Plate 4-1	Plate 4-2	Plate 4-3	Plate 4-4	Plate 4-5
Frequency, Hz	f_1	11580	11653	11435	11580	11435
	f_2	12740	12740	12668	12740	12595
	f_3	15278	15350	15060	15278	15133
	f_4	17380	17380	17090	17235	17163
	f_5	22093	22093	21658	22165	21803
	f_6	38623	38550	38188	38550	37970

The assignment of these designations is based on the work of Zagrai and Giurgiutiu (2001), in which the modeshapes of circular plates in this frequency band were studied theoretically and compared with experimental results. Figure 6 indicates that the flexural modes AF1–AF4 are very strongly excited, as expected in this frequency band. The radial mode AR1 is also excited, but not as strongly. The parasitic non-axisymmetric modes NA1–NA3 are inadvertently excited but with less intensity than the axisymmetric modes.

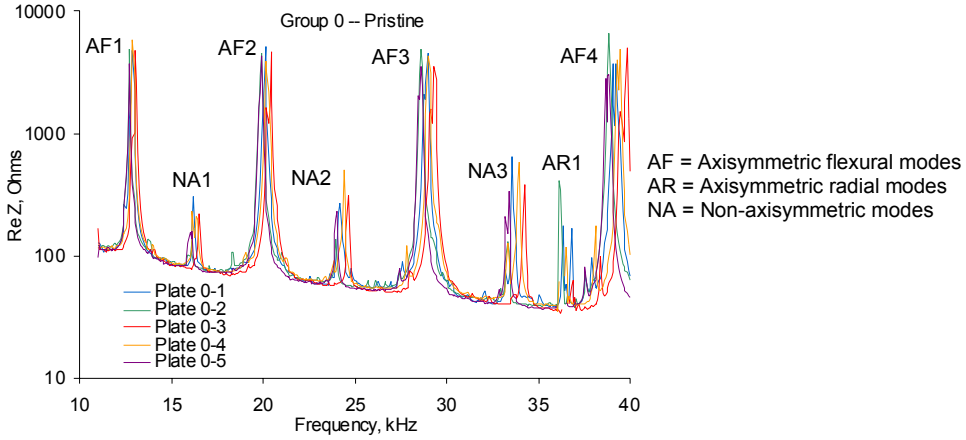

Figure 6 Statistical effects on the impedance spectrum: superposed spectra of the five "identical" Group 0 (pristine) specimens, in the 10–40 kHz band.

The average and standard deviation (STD) values for the resonance frequencies and amplitudes were calculated for all these modes (Table 1). It is noted that the resonant frequencies fall in a very tight interval (1% STD), indicating good experimental reproducibility. It is also noted that the resonance amplitudes show a much wider spread than the frequencies (10–30% STD). This is to be expected considering that the modal amplitudes are affected by the modal damping, which is much more difficult to control than the modal frequencies. However, when the log-amplitudes were considered, the spread reduced considerably (~2% for the main modes AF1, AF2, AF3; more for the other). It is noted that the use of log-amplitude is consistent with the standard practice in experimental modal analysis. For the damage cases (groups 1 through 4), similar results were obtained. These observations were also noted in the higher frequencies bands, 10–150 kHz and 300–450 kHz.

Table 2 Summary of the statistical results for Group 0 (pristine) circular plate specimens: average values and standard deviation (STD) of the frequencies and amplitudes in the lower frequency band (10 – 40 kHz).

Mode type	Frequency			Amplitude			Log-amplitude		
	Average	STD		Average	STD		Average	STD	
	kHz	kHz	%	Ohms	Ohms	%	Log-Ohms	Log-Ohms	%
AF1	12.86	0.12	0.94%	4837	756	15.6%	0.07	0.07	1.87%
NA1	16.22	0.17	1.05%	209	68	32.8%	0.15	0.15	6.35%
AF2	20.11	0.21	1.04%	4491	478	10.6%	0.05	0.05	1.26%
NA2	24.25	0.27	1.11%	291	135	46.5%	0.21	0.21	8.48%
AF3	28.91	0.30	1.05%	4160	598	14.4%	0.06	0.06	1.76%
NA3	33.72	0.40	1.18%	415	203	49.1%	0.28	0.28	10.84%
AR1	36.45	0.29	0.78%	210	122	58.3%	0.22	0.22	9.46%
AF4	39.17	0.30	0.76%	3933	1930	49.1%	0.24	0.24	6.91%

Legend: AF = Axisymmetric flexural modes
AR = Axisymmetric radial modes
NA = Non-axisymmetric modes

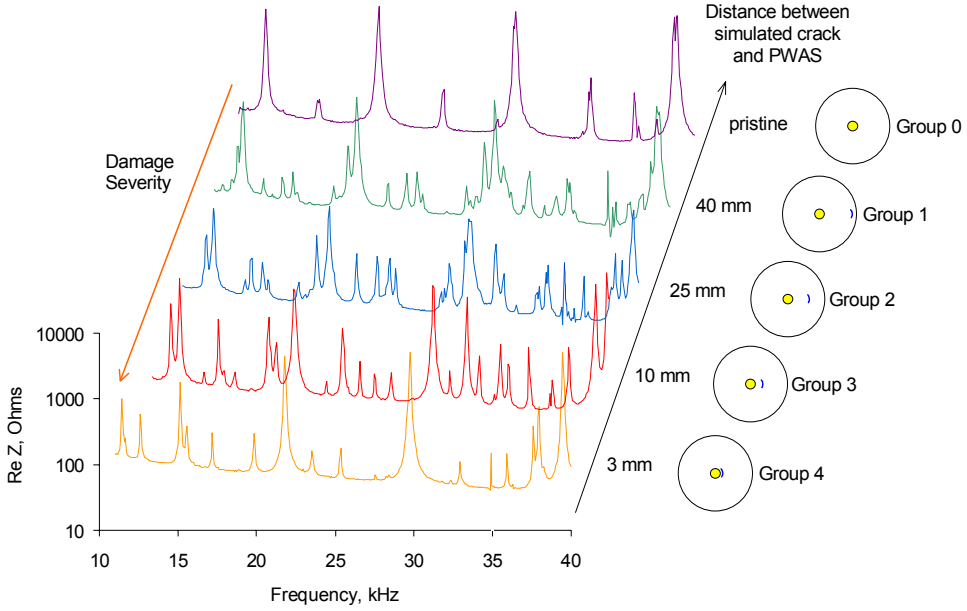

Figure 7 Modification of the impedance spectra with the appearance and location of damage in the 10–40 kHz band

4.2 Damage-Induced Changes in the Impedance Spectra

Figure 7 illustrates how the appearance and progression of damage affects the impedance spectra. The pristine plate had clearly defined sharp resonance peaks, as presented in the top spectrum of Figure 7. The appearance of minor damage (simulated crack located at 40 mm from the PWAS) modified slightly the frequency spectrum by:

(i) Small shifts in the existing resonance peaks
(ii) New low-intensity resonance peaks

However, as long as the damage is minor, the main aspect of the original spectrum is still preserved. As the severity of damage increases (location of simulated crack at 25 and 10 mm from the PWAS), the changes in the spectrum became more drastic, and we noticed:

(i) Large shifts in the existing resonance peaks
(ii) Strong new resonance peaks
(iii) Peak splits

Thus, when the damage is slight, the differences between the pristine spectrum and the damage spectrum are noticeable but slight, whereas when the damage is severe, the differences are very intense. **One challenge in the spectral classification** is to detect not only the intense differences, but also the slight differences. Thus, the better the detection method is, i.e., the better the detection sensitivity, the sooner one would be able to detect incipient damage. **Another challenge** is to avoid false positives, i.e., to avoid signaling damage when no damage is present. False positives may appear due to the statistical variations in impedance reading, which originate either in structural variations, or in sensor installation variations. A good spectral classification would reject these statistical variations and would be sensitive to only the damage effects.

5. APPLICATION OF THE FEATURES-BASED PNN CLASSIFICATION

Features extraction reduces the problem dimensionality and separates essential information from non-essential information. In spectral analysis, the features-vector approach recognizes that the number and characteristics of resonance peaks play a major role in describing the dynamic behavior of the structure. By considering the essential features of the spectrum, i.e. the peaks at resonance frequencies, meaningful information corresponding to the particular state of structural health can be extracted. This information can be organized in a features vector, where each feature corresponds to a certain resonance frequency. As an illustration, consider the E/M impedance spectra reproduced in Table 4b. Each spectrum contains 401 data points positioned at 0.075 kHz intervals in the 10 to 40 kHz band. Five spectra are presented: one pristine and four with various degrees of damaged. Although the difference between spectra is apparent, quantification of this difference is neither obvious nor immediate. Using the features

vector approach, it is possible to distinguish between a "pristine" and a "damaged" structure by considering the number and the position of the resonance peaks. For example, the pristine-plate spectrum of Table 4b displays four dominant resonance peaks (12.8, 20.1, 28.9, and 39.2 kHz), and several minor peaks (16.2, 24.2, 33.7, 36.4 kHz). By considering these features, the dimensionality of the problem can be reduced by almost 2 orders of magnitude, from 400-points to less than 10 features. The details for these feature vectors are given in Table 1c. For the 'strong damage' plate (Table 1, Group 4), we distinguish six dominant peaks (11.6, 12.7, 15.2, 17.4, 22.0, 38.6 kHz). Though the number of features has increased, the problem size is still one order of magnitude less than in a featureless approach. Similar results were also observed in the 10–150 kHz and 300–450 kHz bands.

Once the feature vectors are established, the classification problem can be approached in the features space. Several features-based classification algorithms are possible. We explored a probabilistic neural network (PNN) classification algorithm. The results of our tests are given in Tables 3 and 4. Table 3 shows the PNN classification performed with a 4-frequency features vector. The 4 frequencies used in the features vector were the main resonance frequencies of Table 1c. The results of Table 5 indicate that good classification was attained for Groups 2, 3, 4, but not for Group 1. Group 1 (slight damage) was misclassified with Group 0 (pristine). This misclassification problem could not be fixed by increasing the number of training vectors (Tests II, III, and IV in Table 3). However, when the size of the features vectors was increased from four to six, the classification improved dramatically (Table 4). With only one vector used for training in each group, the PNN consistently predicted the right results. Thus, clear distinction could be established between the spectra generated by the 'pristine' case (Group 0) and the 'damage' cases (Groups 1, 2, 3, 4). In addition, clear distinction could also be determined among the spectra of various 'damage' groups that correspond to various crack positions (Group 4, 3, 2, 1 correspond to r = 3, 10, 25, 40 mm, respectively). Similar good results were also obtained features vector increased from 6 to 11.

Table 3 Synoptic classification table for circular plates using 4-frequency feature vectors

		Group 0 (no damage)					Group 1 (r=40 mm)					Group 2 (r=25 mm)					Group 3 (r=10 mm)					Group 4 (r=3 mm)					
Plate #		1	2	3	4	5	6	7	8	9	10	11	12	13	14	15	16	17	18	19	20	21	22	23	24	25	
Test #	I	T	V	V	V	V	T	V	V	V	V	T	V	V	V	V	T	V	V	V	V	T	V	V	V	V	IN
		–	0	1	1	0	–	1	1	1	1	–	2	2	2	2	–	3	3	3	3	–	4	4	4	4	OUT
	II	T	T	V	V	V	T	T	V	V	V	T	V	V	V	V	T	V	V	V	V	T	V	V	V	V	IN
		–	–	1	1	0	–	–	1	1	1	–	2	2	2	2	–	3	3	3	3	–	4	4	4	4	OUT
	III	T	T	T	V	V	T	T	1	1	1	T	V	V	V	V	T	V	V	V	V	T	V	V	V	V	IN
		–	–	–	1	0	–	–	1	1	1	–	2	2	2	2	–	3	3	3	3	–	4	4	4	4	OUT
	IV	T	T	T	V	T	T	T	V	V	V	T	V	V	V	V	T	V	V	V	V	T	V	V	V	V	IN
		–	–	–	1	–	–	–	1	1	1	–	2	2	2	2	–	3	3	3	3	–	4	4	4	4	OUT

Table 4 Synoptic classification table for circular plates using 6-frequency feature vectors

		Group 0 (no damage)					Group 1 (r=40 mm)					Group 2 (r=25 mm)					Group 3 (r=10 mm)					Group 4 (r=3 mm)					
Plate #		1	2	3	4	5	6	7	8	9	10	11	12	13	14	15	16	17	18	19	20	21	22	23	24	25	
Test #	I	T	V	V	V	V	T	V	V	V	V	T	V	V	V	V	T	V	V	V	V	T	V	V	V	V	IN
		–	0	0	0	0	–	1	1	1	1	–	2	2	2	2	–	3	3	3	3	–	4	4	4	4	OUT
	II	V	T	V	V	V	V	T	V	V	V	V	T	V	V	V	V	T	V	V	V	V	T	V	V	V	IN
		0	–	0	0	0	1	–	1	1	1	2	–	2	2	2	3	–	3	3	3	4	–	4	4	4	OUT
	III	V	V	T	V	V	V	V	T	V	V	V	V	T	V	V	V	V	T	V	V	V	V	T	V	V	IN
		0	0	–	0	0	1	1	–	1	1	2	2	–	2	2	3	3	–	3	3	4	4	–	4	4	OUT
	IV	V	V	V	T	V	V	V	V	T	V	V	V	V	T	V	V	V	V	T	V	V	V	V	T	V	IN
		0	0	0	–	0	1	1	1	–	1	2	2	2	–	2	3	3	3	–	3	4	4	4	–	4	OUT
	V	V	V	V	V	T	V	V	V	V	T	V	V	V	V	T	V	V	V	V	T	V	V	V	V	T	IN
		0	0	0	0	–	1	1	1	1	–	2	2	2	2	–	3	3	3	3	–	4	4	4	4	–	OUT

Legend: T = training vector; V = validation vector; IN = input to PNN, OUT = output from PNN

6. SUMMARY AND CONCLUSIONS

This paper has presented an approach to damage metric quantification based on the comparison and classification of high-frequency local impedance spectra achieved with a neural network approach in conjunction with a features extraction algorithm. These methods have been illustrated on experimental data taken on a set of simple-geometry calibration specimens containing controlled damage and built-in statistical variation: a set 25 simple geometry circular plate specimens with various amounts of damage. The set of calibration specimens was partitioned into five damage classes, each class containing five nominally identical members. The high-frequency impedance spectrum of each specimen was recorded using the electro-mechanical impedance technique in conjunction with surface-mounted

piezoelectric-wafer active sensors (PWAS). Three high-frequency bands were used during the experiment, 10–40 kHz, 10–150 kHz, and 300–450 kHz. The high-frequency character of the recorded data ensured high sensitivity to damage presence and location.

The spectral classification was performed with a features-based probabilistic neural network (PNN). The PNN approach was found to be very successful when applied in conjunction with a features-extraction algorithm. Features-vectors based on the resonance frequencies, resonance amplitudes, and damping factors were identified as possible candidates. In our work, we were able to perform successful classification based on resonance frequencies vectors only. However, the full complement of features may be necessary in situations that are more complicated. For the 10–40 kHz band, we found that correct classification in the five damage classes can be achieved with as little as six resonance frequency features. However, if the number of features was only four (the major peaks only), the classification of mild damage was found to be deficient. This indicates that if the number of frequency features is insufficient, misclassification may occur. A threshold of the minimum number of features for correct classification may exist. Increasing the number of features from six to eleven was also studied. It was found that the eleven-features classification was as good as the six-features classification. For the other frequency bands, which have a higher density of resonance peaks, a larger number of features was necessary. In the 10–150 kHz band, 22 frequency features were identified. Overall, the PNN approach, when used in conjunction with a featured extraction algorithm, was found successful in achieving the correct spectral classification of damage in controlled experiments. It was also found that the inherent statistical variation between the members of the same damage class do not significantly affect the spectral classification provided a sufficient number of features was selected in the features vector.

The outcome of this study consists in the validation of the concept that probabilistic neural networks in conjunction with a features extraction algorithm can successfully classify high-frequency impedance spectra according to the amount of damage present in the structure, and independent of the inherent statistical variation between members of the same damage class. By performing this study on a controlled set of specimens, a benchmark dataset has been generated that could serve as basis for further studies in spectral classification for damage detection.

7. ACKNOWLEDGMENTS

Partial support from the Department of Energy through the Sandia National Laboratories through contract doc. # BF 0133, from the National Science Foundation through grants NSF #CMS-9908293 and NSF INT-9904493, and participation in the US Air Force Summer Faculty Fellowship Program 2002 are thankfully acknowledged.

8. REFERENCES

Bartkowicz, T. J., Kim, H. M., Zimmerman, D. C., Weaver-Smith, S. (1996) “Autonomous Structural Health Monitoring System: A Demonstration”, Proceedings of the 37th AIAA/ASME/ASCE/AHS/ASC Structures, Structural Dynamics, and Materials Conference, Salt-Lake City, UT, April 15-17, 1996

Bishop, C. M. (1995) Neural Networks for Pattern Recognition, Clarendon Press, ISBN 0-19-853849-9

Boller, C., Biemans, C., Staszewski, W., Worden, K., and Tomlinson, G. (1999) "Structural Damage Monitoring Based on an Actuator-Sensor System", SPIE Smart Structures and Integrated Systems Conference, Newport CA. March 1-4, 1999

Chan, T.H.T, Ni, Y.Q.; Ko, J.M, (1999) “Neural Network Novelty Filtering for Anomaly Detection of Tsing Ma Bridge Cables”, Proceedings of the 2nd International Workshop on Structural Health Monitoring, September 8-10, 1999, Stanford University, Stanford, CA, USA, pp. 430-439

Chang, T.Y.P.; Chang, C.C.; Xu, Y.G.. (1999) “Updating Structural Parameters: an Adaptive Neural Network Approach”, Proceedings of the 2nd International Workshop on Structural Health Monitoring, September 8-10, 1999, Stanford University, Stanford, CA, USA, pp. 379-389

Cowell, R. G.; Dawid, A. P.; Lauritzen, S. L.; Spiegelhalter D. J. (1999) Probabilistic Networks and Expert Systems, Springer-Verlag, 1999

Demuth, H.; Beale, M. (2000) MATLAB Neural Network Tool Box, The Math Works, Inc.; Natick, MA.

Farar, R. C.; Sohn, H.; Fugate, M.L, Czarnecki, J.J (2001) “Statistical Process Control and Projection Techniques for Damage Detection”, Proceedings of the SPIE’s Conference on Advanced Nondestructive Evaluation for Structural and Biological Health Monitoring, March 4-8, 2001, Newport Beach, CA, USA, Vol. 4335, pp. 1-19

Farrar, C.R, Duffey, T.A.; Doebling, S.W.; Nix, D.A. (1999) “A Statistical Pattern Recognition Paradigm for Vibration-Based Structural Health Monitoring”, Proceedings of the 2nd International Workshop on Structural Health Monitoring, September 8-10, 1999, Stanford University, Stanford, CA, USA, pp. 764-773

Fritzen, C.P.; Bohle, K. (1999) “Parameter Selection Strategies in Model-Based Damage Detection”, 2nd International Workshop on Structural Health Monitoring, September 8-10, 1999, Stanford University, Stanford, CA, USA, pp. 901-911

Giurgiutiu, V.; Zagrai, A. (2000) "Characterization of Piezoelectric Wafer Active Sensors", *Journal of Intelligent Material Systems and Structures*, Technomic Pub., USA, Vol. 11, No. 12, December 2000, pp. 959-976

Giurgiutiu, V.; Zagrai, A. N. (2002) "Embedded Self-Sensing Piezoelectric Active Sensors for Online Structural Identification", ASME *Journal of Vibration and Acoustics*, Vol. 124, January 2002, pp. 116-125

Hagan, M. T.; Demuth, H. B.; Beale, M. (1996) Neural Network Design, PWS Publishing Co.; Int. Thompson Publishing

Ho, Y.Q.; Ewins, D.J. (1999) "Numerical evaluation of Damage Index", Proceedings of the 2nd International Workshop on Structural Health Monitoring, September 8-10, 1999, Stanford University, Stanford, CA, USA, pp. 995-1009

Hu, N.; Fukunaga, H. (2001) "Structural Damage Identification Using Piezoelectric Sensors", Proceedings of the SPIE's Conference on Advanced Nondestructive Evaluation for Structural and Biological Health Monitoring, March 4-8, 2001, Newport Beach, CA, USA, Vol. 4335, pp. 371-382

Jin, S.; Livingston, R.A.; Morzougui, D. (2001) "Stochastic System Invariant Spectrum Analysis Applied to Smart Systems in Highway Bridges", Proceedings of the SPIE's Conference on Smart Systems for Bridges, Structures, and Highways, March 4-8, 2001, Newport Beach, CA, USA, Vol. 4330, pp.301-312

Kropas-Hughes, C. V.; Rogers, S. K.; Oxley, M. E.; Kabrisky, M. (2002b) Autoassociative-Heteroassociative Neural Network, United States Patent # US 6,401,082 B1, June 4, 2002.

Kropas-Hughes, C.V.; Perez, I.; Winfree; W. P.; Motzer, W. P.; Thompson, R. B. (2002a) "Vision of Future Directions of NDE Research" in Review of Quantitative Nondestructive Evaluation Vol. 21, ed. by D. O. Thompson and D. E. Chimenti, American Institute of Physics, Vol. 615, 2002, pp. 2042-2051

Lindsay, R.; Buchanan, B. G.; Feigenbaum, E. A.; Lederberg, J. (1980) Applications of Artificial Intelligence for Chemical Inference: the DENDRAL Project, McGraw-Hill, NY

Liu, P.; Sana, S.; Rao, V.S. (1999) "Structural Damage Identification Using Time-Domain Parameter Estimation Techniques", 2nd International Workshop on Structural Health Monitoring, September 8-10, 1999, Stanford University, CA, pp. 812-820

Lloyd, G.M, Wang, M.L. (1999) "Neural Network Novelty Filtering for Anomaly Detection of Tsing Ma Bridge Cables", 2nd International Workshop on Structural Health Monitoring, September 8-10, 1999, Stanford University, CA, pp. 713-722

Loh, C.H.; Huang, C.C. (1999) "Damage Identification of Multi-story Steel Frames Using Neural networks", 2nd International Workshop on Structural Health Monitoring, September 8-10, 1999, Stanford University, Stanford, CA, USA, pp. 390-399

Looney, C. G. (1997) Pattern Recognition Using Neural Networks, Oxford Univ. Press

Lopes Jr.; V.; Park, G.; Cudney, H.; Inman, D. (1999) "Smart Structures Health Monitoring Using Artificial Neural Network", 2nd International Workshop of Structural Health Monitoring, Stanford University, September 8-10, 1999, pp. 976-985.

Manolakis, D. G; Ingle, V. K.; Kogon, S. M. (2000) Statistical and Adaptive Signal Processing, McGraw Hill

Mehrotra, K.; Mohan, C. K.; Ranka, S. (1997) Elements of Artificial Neural Networks, MIT Press, ISBN 0-262-13328-8

Morita, K.; Teshigawa, M.; Isoda, H.; Namamoto, T.; Mita, A. (2001) "Damage Detection Tests of Five-Story Frame with Simulated Damages ", Proceedings of the SPIE's Conference on Advanced Nondestructive Evaluation for Structural and Biological Health Monitoring, March 4-8, 2001, Newport Beach, CA, USA, Vol. 4335, pp. 106-114

Ni, Y.Q.; Jiang, S.F.; Ko, J.M. (2001) "Application of Adaptive Probabilistic Neural Networks to Damage Detection of Tsing Ma Suspension Bridge", Proceedings of the SPIE's Conference on Health Monitoring and Management of Civil Infrastructure System, March 4-8, 2001, Newport Beach, CA, USA, Vol. 4337, pp. 347-356

Nigrin, A. (1993) Neural Networks for Pattern Recognition, MIT Press, ISBN 0-262-14054-3

Omidvar, O.; Dayhoff, J. (Eds.) (1998) Neural Networks and Pattern Recognition, Academic Press

Principe, J. C.; Euliano, N. R.; Lefebvre, W. C. (2000) Neural and Adaptive Systems: Fundamentals through Simulation

Shotliffe, E. H.; Buchanan, B. G. (1975) MYCIN: Computer-Based Medical Consultations, Elsevier, NY

Sohn, H.; Farar, R. C. (2000) "Statistical Process Control and Projection Techniques for Damage Detection", European COST F3 Conference on System Identification & Structural Health Monitoring, 2000, Madrid, Spain, pp. 105-114

Sohn, H.; Worden, K.; Farrar, C.R, A. (2001) "Novelty Detection under Changing Environmental Conditions", SPIE's Conference on Smart Systems for Bridges, Structures, and Highways, March 4-8, 2001, Newport Beach, CA, Vol. 4330, pp. 108-127

Todoroki, A.; Shimamura, Y.; Inada, T, (1999) "Plug and Monitor System via Ethernet with Distributed Sensors and CCD Cameras", Proceedings of the 2nd International Workshop on Structural Health Monitoring, September 8-10, 1999, Stanford University, Stanford, CA, USA, pp. 571-580

Tseng, K. K.-H.; Naidu, A. S. K. (2001) "Non-Parametric Damage Detection and Characterization Using Smart Piezoelectric Materials" *Smart Materials and Structures*, Vol. 11, No. 3, pp. 317-329, June 2002

Winston, P. H. (1993) Artificial Intelligence, Addison-Wesley, ISBN 0-201-53377-4

Worden, K. (2000) "Nonlinearity in Structural Dynamics: the Last Ten Years", Proceedings of the European COST F3 Conference on System Identification & Structural Health Monitoring, 2000, Madrid, Spain, pp. 29-51

Worden, K.; Manson, G.; Wardle, R.; Staszewski, W.; Allman, D. (1999) "Experimental Validation of Two Structural Health Monitoring Methods", Proceedings of the 2nd International Workshop on Structural Health Monitoring, September 8-10, 1999, Stanford University, Stanford, CA, USA, pp. 784-799

Ying, Z.G, Ni, Y.Q.; Ko, J.M. (2001) "Seismic Response Mitigation of Adjacent High-Rise Structures Via Stochastic Optimal Coupling-Control", Proceedings of the SPIE's Conference on Smart Systems for Bridges, Structures, and Highways, March 4-8, 2001, Newport Beach, CA, USA, Vol. 4330, pp.289-300

Zagrai, A.; Giurgiutiu, V. (2001) "Electro-Mechanical Impedance Method for Crack Detection in Thin Plates", *Journal of Intelligent Material Systems and Structures,* Vol. 12, No. 10, October 2001, pp. 709-718

Zang, C.; Imregun, M. (2000) "Structural Damage Detection Via Principal Component analysis and Artificial Neural Networks", European COST F3 Conference on System Identification & Structural Health Monitoring, 2000, Madrid, Spain, pp. 157-167